International Journal of Heat and Mass Transfer 52 (2009) 3402–3406

Contents lists available at ScienceDirect

International Journal of Heat and Mass Transfer

journal homepage: www.elsevier.com/locate/ijhmt

Technical Note

A note on laser penetration in nanoshell deposited tissue

Jerry Vera, Yildiz Bayazitoglu *

Department of Mechanical Engineering and Materials Science, Rice University, 6100 Main Street, MS 321, Houston, TX 77005-1892, USA

ARTICLE INFO

Article history:
Received 13 November 2008
Received in revised form 9 February 2009
Accepted 9 February 2009
Available online 26 March 2009

Keywords:
Laser radiation
Cancer therapy
Tissue optics
Hyperthermia
Nanoshells

ABSTRACT

The radiative intensity profiles of biological tissues infused with gold nanoshells and illuminated with collimated radiation are compared. A one-dimensional radiative transport model using the P_1 approximation is used to calculate the collimated and diffuse components of incident radiation in a series of semi-infinite slabs representing nine distinct human tissue media. Each tissue model is subject to 633-nm collimated radiation on one end under four concentrations of nanoshell embedment, with theoretical nanoshells tuned to reach peak absorption at 630 nm. The penetration depth each component is shown to be highly influenced by the base tissue extinction, and the profile morphology can be visibly categorized into one of two groups: low scattering, with scattering coefficients between 4000 and 8000 m^{-1}, and high scattering, with scattering coefficients in the range of 30,000 and 40,000 m^{-1}. Increasing nanoshell density up to 7×10^{16} m^{-3} for both types is shown to decrease penetration depth and lower radiative intensity for the diffuse component while not affecting the penetration depth or intensity of the collimated component.

1. Introduction

Gold nanoshells have the potential to be an incredible asset to photothermal therapy for induced hyperthermia in the treatment of cancers. It has been shown in model and experiment that increased concentrations of gold nanoshell particles in biological tissues exposed to laser radiation lead to shorter heating times and increased precision in the targeting of cancers for therapeutic heating [1,2]. The degree of nanoshell addition necessary for hyperthermia and its effect on light penetration and subsequent heating have also been shown in [1] to be highly dependent on the optical and thermal properties of the host tissue alone. This leads to the need for catering specific therapies for each of the different tissue types, and possibly, tissue lengths needed for a given tumor size.

The purpose of this paper is to illustrate the different radiative intensity profiles resulting from the application of the same collimated laser source to different tissue media. The P_1 approximation of radiative transfer theory is used to take the absorption and scattering properties of a given one-dimensional, gray, participating medium and calculate the collimated and diffuse components of incident radiation resulting from a beam of laser radiation penetrating from one end. The changes in intensity profiles resulting from the addition of nanoshells are also shown for each tissue. These profiles serve to illustrate the relative amounts of incident radiation delivered throughout the tissue by means of continued collimated radiation by the illuminating laser and by diffuse radiation resulting from the outscattering and subsequent inscattering by tissue surrounding the one-dimensional path of study. Knowledge of radiative intensity as a function of depth in the medium is pertinent to any therapy or imaging technique that uses lasers in the human body. Furthermore, a rudimentary understanding of different tissue media, their optical properties, and how these properties comparatively result in different optical penetration is highly advantageous to researchers and oncologists alike.

2. Analysis

Previous studies have shown that the optical properties of a participating medium can be altered by adding a homogenous array of gold nanoshells to its matrix [3]. As light enters a nanoshell-embedded slab, propagating light is absorbed and scattered by both the host medium and the embedded nanoshells. The extent of absorption and scattering made by these two constituents can be analyzed linearly, since radiative transfer theory shows that the radiative intensity of a propagating light through an absorbing and isotropically scattering, one-dimensional plane parallel medium with constant radiative properties is a linear function.

Gold nanoshells have the distinct property of being able to be engineered to exhibit peak absorption or peak scattering at any particular wavelength in the visible or near-infrared range. This tunability is achieved by the modification of the diameter of the silica dielectric core and the thickness of the gold shell surrounding it. When an electromagnetic field strikes these nanoshells, the surface electrons oscillate back and forth, causing instantaneous dipole moments. When the oscillation of the dipoles and electromagnetic field

* Corresponding author. Tel.: +1 713 348 6291.
E-mail address: bayaz@rice.edu (Y. Bayazitoglu).

0017-9310/$ - see front matter © 2009 Elsevier Ltd. All rights reserved.
doi:10.1016/j.ijheatmasstransfer.2009.02.014

Nomenclature

Symbols

C_1	analytical constant (Ref. [3])
C_2	analytical constant (Ref. [3])
B_1	analytical constant (Ref. [3])
G	incident radiation (W/m^2)
G_c	collimated component of incident radiation (W/m^2)
G_d	diffuse component of incident radiation (W/m^2)
I_b	blackbody intensity (W/m^2)
N_T	nanoshell concentration (particles per m^3)
q	heat flux (W/m^2)
q_{in}	input laser power (W/m^2)
$q_{c\lambda}$	spectral collimated heat flux (W/m^2)
$q_{d\lambda}$	spectral diffuse heat flux (W/m^2)
$q_{R\lambda}$	spectral radiative heat flux (W/m^2)
$Q_{\sigma\lambda}$	spectral nanoshell absorption efficiency (m^{-1})
$Q_{\kappa\lambda}$	spectral nanoshell scattering efficiency (m^{-1})
r_i	nanoshell gold layer inner radius (nm)
r_o	nanoshell gold layer outer radius (nm)

Greek symbols

$\kappa_{s\lambda}$	spectral scattering coefficient of nanoshell array (m^{-1})
$\kappa_{md\text{-}\lambda}$	spectral scattering coefficient of host tissue medium (m^{-1})
$\sigma_{s\lambda}$	spectral absorption coefficient of nanoshell array (m^{-1})
$\sigma_{md\text{-}\lambda}$	spectral absorption coefficient of host tissue medium (m^{-1})
ρ	reflectivity
τ	optical depth at optical location
$\omega_{tot\text{-}\lambda}$	spectral scattering albedo
μ_0	cosθ
ζ_1	analytical constant (Ref. [3])

Subscripts

c	correspond to collimated radiation
d	correspond to diffuse radiation
i	correspond to inner dimension
in	correspond to input
md	correspond to host medium
o	correspond to outer dimension
R	correspond to total radiation, summation of diffuse and collimated radiation
s	correspond to nanoshells
tot	correspond to total properties for nanoshell/host medium composite

Greek subscripts

β	correspond to extinction
κ	correspond to absorption
λ	spectral
σ	correspond to scattering

are in resonance, maximum absorption occurs. Nanoshells used for photothermal therapy are tuned to exhibit peak absorption at a wavelength where surrounding tissue exhibits minimal native absorption. The purpose of this is to localize absorption in the areas only where nanoshells are located, primarily the site of a tumor.

The optical properties of tissue – the index of refraction, absorption, scattering, and extinction – are readily available in the literature. Duck conducted an investigation and compiled a comprehensive list of optical, thermal, and other physical properties of a variety of biological tissue media [4]. In the minimal absorption zone, or therapeutic zone, of tissue optics mentioned above, his list includes those optical properties of tissues at 633 nm and others, but does not include a large compilation at 820 nm, where the absolute minimum absorption due to water occurs. For this reason, this investigation will be conducted using scattering and absorption properties of tissues at 633 nm, since tissue absorption is still sufficiently low under this laser. Accordingly, the theoretical nanoshells are tuned for peak absorption at this wavelength. The optical properties of the tissues studied are listed in Table 1 in order of decreasing scattering albedo.

The aspect ratio of the theoretical nanoshells used in this study is $[r_i, r_o] = [16, 21]$-nm. This ratio is found using Mie scattering theory, which has been shown to be a good model of nanoshell optical behavior [5]. The efficiency spectrum of the scattering, absorption, and extinction – their sum – is shown in Fig. 1.

2.1. Nanoshell addition

When nanoshells are added to a tissue matrix, the optical properties of the matrix are altered, with increased alteration in proportion to the number of nanoshells added, the nanoshell cross-sectional area, and the absorption and scattering efficiencies shown in Fig. 1. A multitude of nanoshells added to a given matrix makes up a nanoshell array, which has the following absorption and scattering coefficients:

$$\sigma_{s\lambda} = \pi r_o^2 Q_{\sigma\lambda} N_T \quad (1)$$

$$\kappa_{s\lambda} = \pi r_o^2 Q_{\kappa\lambda} N_T \quad (2)$$

The cross-sections obtained are added to those native optical properties listed in Table 1 for each respective tissue base and one of four nanoshell concentrations of $N_T = 0$, 7×10^{14}, 7×10^{15}, and 7×10^{16} particles per cubic meter. The augmentation to absorption and scattering resulting from their addition to the tissue media is presented in Table 2. The total scattering albedo for the nanoshell-tissue composite is calculated using:

Table 1
Utilized tissue optical properties at 633 nm. Source: [4].

Tissue	Index of refraction	Absorption (m^{-1})	Scattering (m^{-1})	Total extinction (m^{-1})	Scattering albedo
Subcutaneous fat	1.44	10	6690	6700	0.9985
Adult brain gray matter	1.37	26	5700	5726	0.9955
Skeletal muscle	1.37	35	4500	4535	0.9923
Rib bone	1.54	100	4000	4100	0.9756
Breast tissue	1.44	20	39,400	39,420	0.9995
Aortic tissue	1.39	52	31,500	31,552	0.9984
Skin dermis	1.55	180	39,400	39,580	0.9955
Human liver	1.37	320	41,100	41,420	0.9923
Lung tissue	1.38	840	35,900	36,740	0.9771

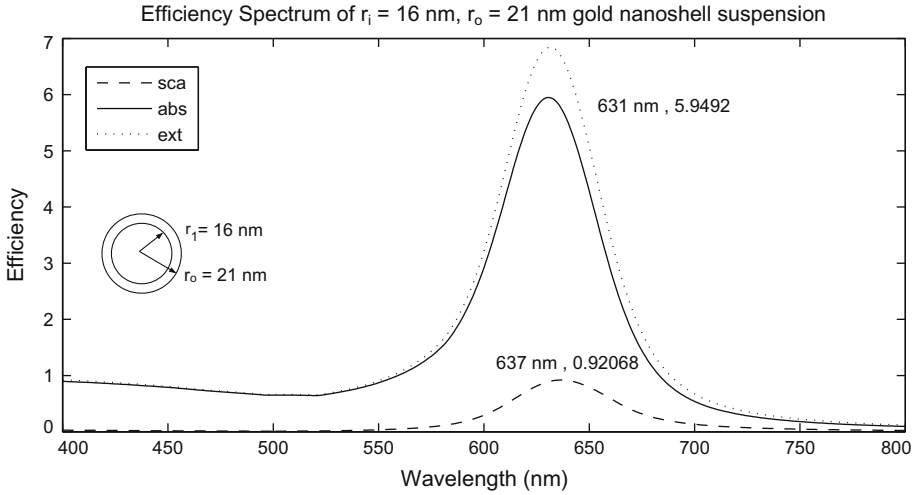

Fig. 1. Scattering and Absorption spectra of $[r_i, r_o] = [16, 21]$-nm nanoshell suspension from Mie theory approximation with line broadening due to polydispersity in shell population.

$$\omega_{tot-\lambda} = \frac{\sigma_{s\lambda} + \sigma_{md-\lambda}}{\pi r_o^2 Q_{\kappa\lambda} N_T + \pi r_o^2 Q_{\sigma\lambda} N_T + \kappa_{md-\lambda} + \sigma_{md-\lambda}} \tag{3}$$

where the subscript *md* refers to those properties belonging to the base tissue medium, and the subscript *s* to properties of the nanoshell array.

2.2. P_1 approximation

In [6], Modest describes how the diffuse incident radiation profile as a function of optical depth inside a one-dimensional, semi-transparent, participating medium can be approximated using the P_1 approximation, shown below.

$$\frac{dq}{d\tau} = (1 - \omega_{tot-\lambda})(4\pi I_b - G), \quad \frac{dG}{d\tau} = -3q \tag{4}$$

The incident radiation, $G(\tau)$, is that radiation which enters a single point from all directions, and it is the subject of investigation in this study. It includes both the collimated radiation from the entry direction and the omnidirectional diffuse radiation created through the outscattering from the immediate surroundings. It is calculated by solving Eq. (4). In order to do this, the spectral radiative heat flux, $q_{R\lambda}(\tau)$, is first solved. This is done by the decomposition of its components into collimated and diffuse by the following relation:

$$q_{R\lambda}(\tau) = q_{c\lambda}(\tau) + q_{d\lambda}(\tau) \tag{5}$$

The collimated component is derived as a function of input power, reflectivity, and incoming direction:

$$q_{c\lambda}(\tau) = (1 - \rho) q_{in} e^{\frac{-\tau}{\mu_0}} \tag{6}$$

where μ_o is the directional cosine and is equal to 1 for a laser beam normal to the boundary. The diffuse component is given as

$$q_{d\lambda}(\tau) = C_1 e^{\check{\varsigma}_1 \tau} + C_2 e^{-\check{\varsigma}_1 \tau} + B_1 e^{-\tau} \tag{7}$$

where C_1 and C_2 are analytical constants which can be found in [3]. Using these results, the diffuse heat flux is then calculated, and its derivative with respect to the optical depth is used below to solve for the diffuse component of incident radiation:

$$G_d(\tau) = \frac{1}{1 - \omega}\left(-\frac{dq_d}{d\tau} + \omega(G_c(\tau))\right) \tag{8}$$

where the collimated component of the incident radiation is equivalent to the collimated heat flux given in Eq. (6):

$$G_c(\tau) = (1 - \rho) q_{in} e^{-\tau} \tag{9}$$

3. Results

The incident radiation profiles of nine tissues resulting from a 10,000 W/m^2 exposure are presented in Fig. 2. Here the intensity is measured in a non-dimensional term, $\Phi(\tau_\lambda)$, composed of the ratio of the local incident radiation divided by the input laser power. The tissues are ordered in order of similarity in shape and length of optical penetration.

Upon initial inspection, we see that subcutaneous fat, adult brain gray matter, skeletal muscle, and rib bone, (a)–(d), each have moderately broad profiles, exhibit a peak intensity within the first millimeter, and then drop off gradually to zero. Each tissue in this group has a scattering coefficient in the range of 4000–7000 m^{-1}, with subcutaneous fat having the highest scattering coefficient at 6690 m^{-1} and rib bone having the lowest scattering coefficient at 4000 m^{-1}. This group shall be collectively referred to as *low scattering tissues*.

Another item of importance is to note the relative effects of increased absorption. Absorption increases from 10 to 100 m^{-1} from subcutaneous fat to rib bone. Although it is not immediately clear whether the decrease in intensity between these tissues is due to

Table 2
Contribution to absorption and scattering by $[r_i, r_o] = [16, 21]$-nm nanoshells.

Dispersion density (m^{-3})	Nanoshell area (m^2)	Absorption efficiency (m^{-1})	Scattering efficiency (m^{-1})	Shell absorption coefficient (m^{-1})	Shell scattering coefficient (m^{-1})
0	1.38544E-15	5.9492	0.92968	0	0.000
7.00E + 14	1.38544E-15	5.9492	0.92968	5.770	0.902
7.00E + 15	1.38544E-15	5.9492	0.92968	57.696	9.016
7.00E + 16	1.38544E-15	5.9492	0.92968	576.959	90.161

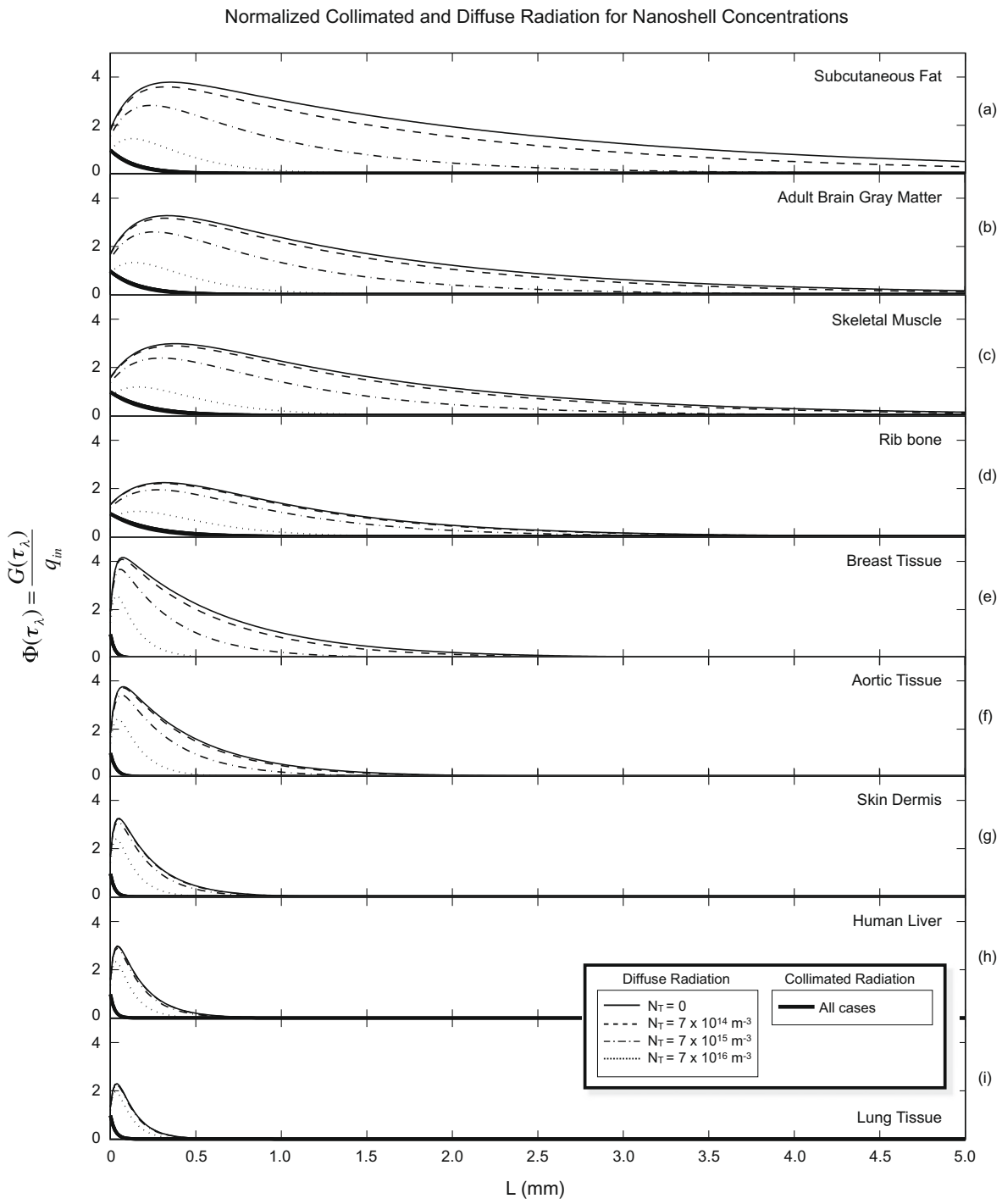

Fig. 2. Normalized collimated and diffuse radiation for nanoshell concentrations for nine tissues, ordered by decreasing penetration depth.

the decrease in scattering or the increase in absorption between them, the changes resulting from increase in nanoshell concentration gives us more insight. Because the nanoshells are tuned to increase absorption with relatively minor effects on scattering, the increased concentrations results in an overall increase in absorption in the tissue composite while holding the total scattering relatively constant. We see from the figure that increased nanoshell concentration creates a less intense (decrease in intensity), less penetrating profile. We also see that subcutaneous fat with $N_T = 7 \times 10^{15}$ nanoshells/m^3 has a very similar profile to skeletal muscle with a higher inherent absorption but no nanoshells at all. This leads to the conclusion that the change in absorption is mostly responsible for the decreased intensity and penetration depth observed. The increase in absorption also results in the increase of extinction and the decrease of scattering albedo.

Breast tissue, aortic tissue, skin dermis, liver, and lung tissue, shown in profiles (e)–(i), exhibit different behavior. The overall shape of the profiles are different, and this group exhibits a slightly higher initial intensity in a peak slightly closer to the entry region with a much steeper subsequent drop off of intensity to zero going into their depths. Compared to the previous tissue set, the scattering coefficients of these tissues range between 31,500 and

41,100 m^{-1}, with an average approximately 7 times greater. This set of tissues is thus collectively referred to as *high scattering tissues*.

The addition of nanoshells in both cases show a preservation of the same profile outline, creating contour-like levels of incident radiation that subsequently decrease in intensity, shifts the peaks slightly closer to the entry, and also shifts the point of complete extinction closer the entry zone as nanoshell concentration rises. However, this noteworthy change in light behavior only occurs in the diffuse component. With each tissue specimen, the addition or increase of nanoshells has little to no noticeable affect on the collimated radiation. The profiles of the collimated component in all four low scattering tissues are nearly identical among one another and remain identical individually despite nanoshell addition within each tissue. Likewise, the profiles of the collimated components in the five high scattering tissues are also identical to one another and are virtually unaltered with the addition of nanoshells in the degree of addition presented here.

Despite this inalterable behavior, the collimated curves do notably differ between the low scattering group and the high scattering group. In the tissues with lower scattering, the length to extinction is approximately 0.5 mm. The higher scattering group has a shorter length of extinction at approximately 0.1 mm. At this point, all collimated rays are either fully absorbed or fully scattered away, and the remaining intensity is due to the outscattered diffuse radiation that scatters back into the path of observation from the immediate surroundings. This inscattering is also subject to further outscattering and absorption, then subsequent inscattering, absorption, and outscattering again until all remaining radiation is absorbed or scattered completely away.

Upon inspection of Table 1, we see that the scattering albedos of all tissue here is high, ranging from a low of 0.9771 to a high of 0.9985 before nanoshell embedment. These high values (values close to one) indicate that the dominant mode of radiative transport is scattering, and diffuse radiation should be highly active as a result. Fig. 2 supports this conclusion. While the addition of nanoshells increases absorption and decreases the overall scattering albedo, we see that this decrease isn't sufficient to significantly alter the shape of the collimated radiation curve even after adding concentrations as high as $N_T = 7 \times 10^{16}$ nanoshells/m^3. We do clearly see its effect on the diffuse component, however.

Finally, one should take note that the phenomena described above and the order shown in Fig. 2 can be predicted when considering the scattering coefficients and scattering albedos of the host media. When the tissues listed in Table 1 are ordered first based on scattering group, with low scattering followed by high scattering, then in order of decreasing scattering albedo, we see that the order matches that shown in the figure, which is ordered by decreasing length for total extinction. It is interesting to note that while this study concentrates on the effects of nanoshell addition for absorption-enhancing nanoshells, strictly from the standpoint of altering the tissue data in Table 1, we can see that adding scattering-enhancing nanoshells may also produce dramatic effects in the intensity profile similar to the differences between the high and low scattering tissue groups. However, in order to produce this class of alteration, the augmented scattering coefficient of the nanoshell array – produced by Eq. (2) – would have to be in the order of $\sim$28,000 m^{-1}, a factor much greater than the maximum absorption produced by the highest concentrated absorption-enhancing nanoshell array in this study. Scattering-enhancing nanoshells used for this purpose would have to exhibit peak scattering at or near 633-nm and likely require a dispersion density an order of magnitude higher than the maximum used for absorption in Table 2. However, the need for higher dispersion may be slightly reduced due to the larger cross-sectional area produced by light-scattering nanoshells, which would likely be larger in diameter.

4. Conclusion

The one-dimensional radiative intensity profiles of nine tissues following identical exposure to collimated radiation have been simulated using a P_1 approximation-based code. Of the tissues presented, four exhibit optical properties characterizing them as low scattering, and five possess optical properties characterizing them as high scattering. It has been shown that the low scattering tissues exhibit a broad, lengthened penetration profile with decreasing intensity and penetration depth corresponding to decreasing scattering albedo. High scattering tissues exhibit a less broad penetration profile, dominated by a sharp peak near the entry and followed by a quick fall down to total extinction near or within 2 mm. It is also shown that adding nanoshells tuned to enhance absorption in the matrix, as would be done during photothermal cancer therapy, significantly alters the diffuse component of radiation while not affecting the collimated component. For both low and high scattering sets, the addition of nanoshells decreases the relative intensity, shifts the peak of highest intensity slightly closer to the entry region, and significantly shortens the length required for full extinction. This effect increases with increasing nanoshell concentration.

Finally, it is shown that scattering plays a dominant role in radiative transport for tissues, and as a result, diffuse radiation is dominant over collimated radiation, which becomes extinct within the first millimeter of penetration. Any calculations attempting to omit diffuse radiation and only use collimated radiation due to its simplicity would be insufficient for a complete radiative profile.

Acknowledgements

This work was funded by the Alliances for Graduate Education and the Professoriate (AGEP) program through the National Science Foundation Grant HRD-0450363.

References

[1] J. Vera, Y. Bayazitoglu, Gold nanoshell density variation with laser power for induced hyperthermia, Int. J. Heat Mass Transfer 52 (2009) 564–573.
[2] L.R. Hirsch, R.J. Stafford, J.A. Bankson, S.R. Sershen, B. Rivera, R.E. Price, J.D. Hazle, N.J. Halas, J.L. West, Nanoshell-mediated near-infrared thermal therapy of tumors under magnetic resonance guidance, PNAS 100 (2003) 13549–13554.
[3] I. Tjahjono, Y. Bayazitoglu, Near-Infrared light heating of a slab by embedded nanoparticles, Int. J. Heat Mass Transfer 51 (2008) 1505–1515.
[4] Francis A. Duck, Physical Properties of Tissue: A Comprehensive Reference Book, Academic Press Inc., San Diego, 1990.
[5] E. Prodan, P. Nordlander, Plasmon hybridization in spherical nanoparticles, J. Chem. Phys. 120 (11) (2004) 5444–5454.
[6] M. Modest, Radiative Heat Transfer, second ed., Academic Press, New York, 2003.